Optically switchable organic light-emitting transistors

Lili Hou[1], Xiaoyan Zhang[1,4], Giovanni F. Cotella[2], Giuseppe Carnicella[2], Martin Herder[3], Bernd M. Schmidt[3], Michael Pätzel[3], Stefan Hecht[3,*], Franco Cacialli[2,*], Paolo Samorì[1,*]

1 Université de Strasbourg, CNRS, ISIS, 8 alleé Gaspard Monge, 67000 Strasbourg, France. Email: samori@unistra.fr

2 Department of Physics and Astronomy (CMMP Group) and London Centre for Nanotechnology, University College London, Gower Street, London WC1E 6BT, United Kingdom. Email: f.cacialli@ucl.ac.uk

3 Department of Chemistry & IRIS Adlershof, Humboldt-Universität zu Berlin, Brook-Taylor-Str. 2, 12489 Berlin, Germany. Email: sh@chemie.hu-berlin.de

4 Present address: Department of Chemistry and Chemical Engineering, Chalmers University of Technology, 412 96 Gothenburg, Sweden.

Organic light-emitting transistors (OLETs) are pivotal components for emerging opto- and nano-electronics applications, such as logic circuitries and smart displays. Within this technology sector, the integration of multiple functionalities in a single electronic device remains the key challenge. Here, for the first time, we have fabricated optically switchable organic light-emitting transistors (OSOLETs) through a judicious combination of light-emitting semiconductors and photochromic molecules. The irradiation of the solution-processed films at selective wavelengths enables the efficient and reversible tuning of charge transport and electroluminescence simultaneously, with a high degree of modulation (on/off ratios up to 500) in the three primary colors. Different emitting patterns can be written and erased, through a non-invasive and mask-free process, on a length scale of few microns in a single OSOLET, thereby rendering our devices of interest for optically gated highly-integrated full-color displays and active optical memory technologies.

Organic light-emitting transistors (OLETs), combining in a single device the functions of light generation of organic light-emitting diodes (OLEDs) with the current modulation (and signal amplification) of organic thin-film transistors (OTFTs), have emerged as a promising new class of devices with significant potential for integrated optoelectronics, smart display technology, and organic lasers[1-5]. The emitting layer of the unencapsulated OLETs is easily accessible for comprehensive optical and electrical investigation of the fundamental physical processes, thereby providing powerful insights into device physics[6,7]. The architecture and ease of fabrication of

OLETs potentially omit multi-step metal and materials evaporation that might damage the interface between electrodes and active layers, greatly simplifying the device architecture and thereby enabling its potential use in active matrix displays. Furthermore, the position of the recombination region in the channel of ambipolar OLETs can be shifted away from the electrodes as a function of the applied bias, avoiding the metal-induced quenching of excitons[8-10]. Capelli *et al.* recently demonstrated that the performance of OLET can be boosted by exploiting a trilayer heterostructure, surpassing the equivalent OLED efficiency over 100 times[11]. OLETs comparable to display pixels driven by polycrystalline-silicon backplane transistors have been reported, which can be operated at low-voltage and low-power consumption[12].

Beside the efforts to enhance the charge carrier mobility, efficiency, and brightness of OLETs[13-16], the integration of further functionalities into a single device represents another important challenge with the prospect of realizing controllable integrated circuitry[17,18]. Electrically switchable chiral light-emitting transistors (LETs) have been demonstrated, in which the current direction can be used to control the polarization of light from *pn* junctions in tungsten diselenide (WSe_2), which serves as a channel material of LETs[19]. Another example is an all-graphene based light-emitting field-effect device featuring an external electrical bias tuning of the emission spectrum[20]. However, these multifunctional LETs, based on two-dimensional (2D) materials differ in terms of the nature of the charge transport and mechanism of light

generation compared to OLETs. The current approach to control "multifunctional" LETs still relies on external electrical driving. Conversely, optical control offers various advantages, such as non-invasivity, high spatial and temporal resolution, and the possibility to tune both wavelength and intensity of the emitted light[21].

Some of us recently demonstrated that it is possible to fabricate optically switchable multifunctional OTFTs[22-24], by blending organic semiconductors with photochromic diarylethenes (DAEs). Upon exposure to light of different wavelength，DAEs can be toggled between two isomers with different electronic properties, and they also show high thermal stability and fatigue resistance during continuous photoswitching[25-27]. Such optically responsive OTFTs exhibited high current switching ratios and large charge carrier mobilities, and have been applied for the fabrication of flexible non-volatile optical memory with over 256 distinct levels[28].

Here we report the fabrication and characterization of the first optically switchable organic light-emitting transistors (OSOLETs), by integrating DAEs into the light-emitting semiconducting layer of OLETs *via* simple solution processing. Both charge transport and electroluminescence (EL) are simultaneously modulated by irradiating the devices at distinct wavelengths. We demonstrate three classes of OSOLETs emitting over the entire visible spectrum (green, red, and blue), which can reversibly and remotely switch charge transport and EL on and off *via* visible and UV light irradiation. In addition, emitting patterns within one pixel of the OSOLET can be

written and erased easily by using a light beam as an external, non-invasive, and mask-free writing tool with a spatial resolution down to the far-field diffraction limit, i.e. $\lambda/2NA < 1$ µm (with λ being the wavelength of visible light and NA the numerical aperture of the optical tool used). In view of current minimum pixel sizes, e.g. in the best "retina" displays (~55.5 µm), the present system holds particular potential of reversibly encoding high-density visual information into a single pixel of a high-resolution display.

Results and discussion

Three commercially-available semiconducting light-emitting polymers poly(9,9-dioctylfluorene-*alt*-bithiophene) (F8T2), poly[2-methoxy-5-(3',7'-dimethyloctyloxy)-*para*-phenylenevinylene] (MDMO-PPV), and poly(9,9-dioctylfluorene) (F8) were used to fabricate OLETs having fluorescence emission ranging from blue to red (Fig. 1a), thus covering the entire visible spectrum (supplementary Fig. S1 for the absorption and photoluminescence (PL) spectra). To enable the optical switching in OLETs, an energetic matching between the photochromic molecules and the emissive materials is required, i.e., the highest occupied molecular orbital (HOMO) levels of the emissive polymers should energetically be positioned in between those of the open and closed DAEs (Fig. 1b). According to cyclic voltammetry (CV) measurements of the light-emitting polymers (see supplementary Fig. S2) and previous studies on DAEs[23,29,30], the HOMO levels of DAEs in their open forms are slightly below the one of the green and blue-emitting hosts (~100 meV) and comfortably below that of MDMO-PPV (~200 meV).

Conversely, the HOMO levels of the DAEs in their closed forms are > 600 meV higher than the HOMO of the light-emitting polymers in all three binary components, and thus significant hole trapping is expected for the DAEs in their closed form. In view of the different HOMO levels of the three polymers responsible for red, green, and blue light emission, we have selected two DAEs, i.e., DAE_tBu and DAE_F (Fig. 1a)[29,30] having high fatigue resistance over repetitive photoswitching cycles in the solid state (Fig. S4). Based on the energetic considerations above, DAE_tBu molecules act as switchable charge traps within the matrix of the emissive F8T2 and MDMO-PPV, whereas the lower HOMO level of DAE_F makes it suitable in combination with the blue emitter (F8).

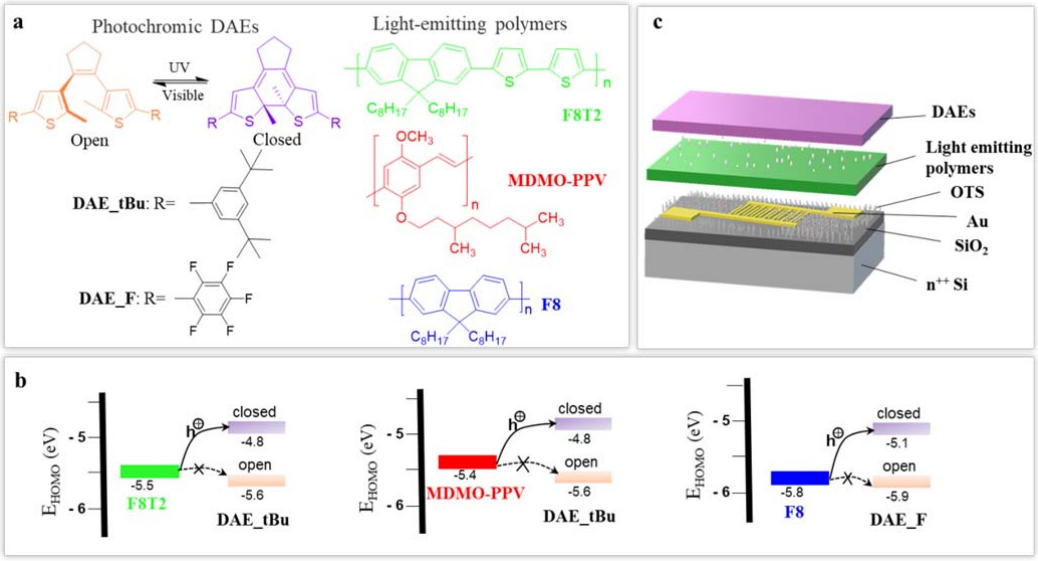

Fig. 1 | Molecules, energetics, and device structure of OSOLETs. a, Chemical structures of photochromic diarylethenes (DAE_tBu and DAE_F) and light-emitting polymers (green: F8T2; red: MDMO-PPV; blue: F8). **b**, Schematic illustration of the switchable charge trapping mechanism of OSOLETs based on the HOMO energy levels of DAEs. As an illustrative example, for F8T2, its hole transport is greatly favoured to the closed form of DAE_tBu but not to the open form of the latter. Thus, there is minimal trapping for the open form, while it is significant for the closed form of DAE_tBu. **c**, Structure of the OSOLETs (substrate, dielectric layer, source and drain electrodes are the same for all the devices, while the light-emitting polymers and

DAEs are varied).

The OSOLETs were fabricated in a bottom-gate bottom-contact configuration with SiO_2/Si as substrates and the pre-patterned gold interdigitated electrodes as source and drain contacts (Fig. 1c, see supplementary information for details). To enhance the charge carrier mobility, self-assembled monolayers (SAMs) of octadecyl-trichlorosilane (OTS) were chemisorbed onto the SiO_2/Si substrates[31,32] prior to spin-coating the solutions of the light-emitting polymers, followed by their thermal annealing at 170 □ to leverage their optoelectronic properties.[33] To avoid thermal degradation of the DAEs at such high temperature, the photochromic molecules were dissolved in solvents orthogonal to those used for the polymers and spun on top of the emissive layer. A gentle post-annealing process was applied to activate the thermal diffusion of DAE molecules into the polymer matrix (80 □ for 1 h in the case of F8T2 and MDMO-PPV, while 40 □ for 1.5 h with regards to F8). The morphologies of the deposited light-emitting polymer/DAE bicomponent films were investigated by atomic force microscopy (AFM, see supplementary Fig. S3). The deposition of DAE_tBu *via* this permeation process did not modify the morphology of F8T2 and no phase separation was observed. Only minor morphology variations were monitored in the case of MDMO-PPV. However, the exposure of neat F8 to both the solvent and thermal treatment, helps the diffusion of DAE_F into F8, and further promotes the formation of supramolecular structures (such as the crystalline phase[34] and the conformational isomer β-phase[35]) of F8, resulting in a rougher morphology (from R_{rms} = 3.0 nm for the neat F8 film to R_{rms} = 12.3 nm for

146 the F8/DAE_F film) due to the presence of micron-sized islands from the
147 aggregation[36].
148
149 We assessed the retained photoisomerization ability of DAEs in the solid state in
150 the presence of the selected light-emitting polymers for the OSOLETs. UV/visible
151 absorption spectroscopy on the light-emitting polymer/DAE bicomponent films
152 revealed upon UV (312 nm) irradiation the appearance of the typical spectral features
153 in the visible region for the closed DAE isomer that disappear upon green light (> 520
154 nm) irradiation (see supplementary Fig. S5). These observations provide unambiguous
155 evidence that after diffusion into the three polymer matrices the DAEs are still able to
156 undergo reversible photoisomerization.
157
158 The performance of OSOLETs in the three primary colors was characterized by
159 using EL spectroscopy as well as transfer curves of current density and luminance *vs.*
160 gate voltage, as summarized in Fig. 2. The light generated within the channel was
161 observed when OSOLETs were in operation, and thereby EL spectra and optical
162 images (inset) of the green, red and blue OSOLETs (channel length L = 2.5 μm and
163 channel width W = 1 cm) were recorded (Fig. 2a-c). The emission peaks of the green
164 and red OSOLETs are located at 540 nm (FWHM = 90 nm) and 630 nm
165 (FWHM = 143 nm), respectively. Two emissive bands appear in the F8/DAE_F based
166 OSOLET with the main peak at 450 nm. The red-shift of EL spectra, compared to that
167 of glassy F8 film with the S_1 to S_0 vibronic peaks at 420 nm, suggests a high fraction

168 of β-phase chain conformations in the F8/DAE_F binary component film[35].
169 Furthermore, we note the presence of an emission band at longer wavelengths, i.e. a
170 green band, which is common in F8-based emissive devices due to the formation of
171 inter-chain states and/or fluorenone defects[37-40]. Importantly, the emissive bands of the
172 three OSOLETs cover well both the visible region (400-700 nm) and even stretch into
173 the near infrared (NIR) up to 800 nm.
174
175 Although light emission requires bipolar injection, most of the transport of our
176 OSOLETs can be described as essentially unipolar, as inferred from the dependence
177 of the drain current on the applied gate voltage, in line with previous literature on
178 non-switchable OLETs[41-43]. While the holes are evenly distributed within the device
179 channel, light emission provides indeed evidence for electron injection and diffusion
180 ranging to several nm inside the channel. Yet electrons remain minority carriers up to
181 the highest (gate and drain) voltages tested here, as their contribution to the overall
182 current is never appreciable. Because of this reason, electron transport and light
183 modulation thereof cannot be determined by using the chosen materials (lowest
184 unoccupied molecular orbital (LUMO) levels listed in Scheme S1). The
185 corresponding light is emitted closely to the electrode in F8T2 based OLET with a
186 longer channel width (L = 20 μm) (see supplementary Fig. S6). However, owing to
187 the resolution of our camera and the narrow channel width of the OSOLETs, the light
188 emission was observed over the entire channel area in the optical images (Figs. 2a-c).

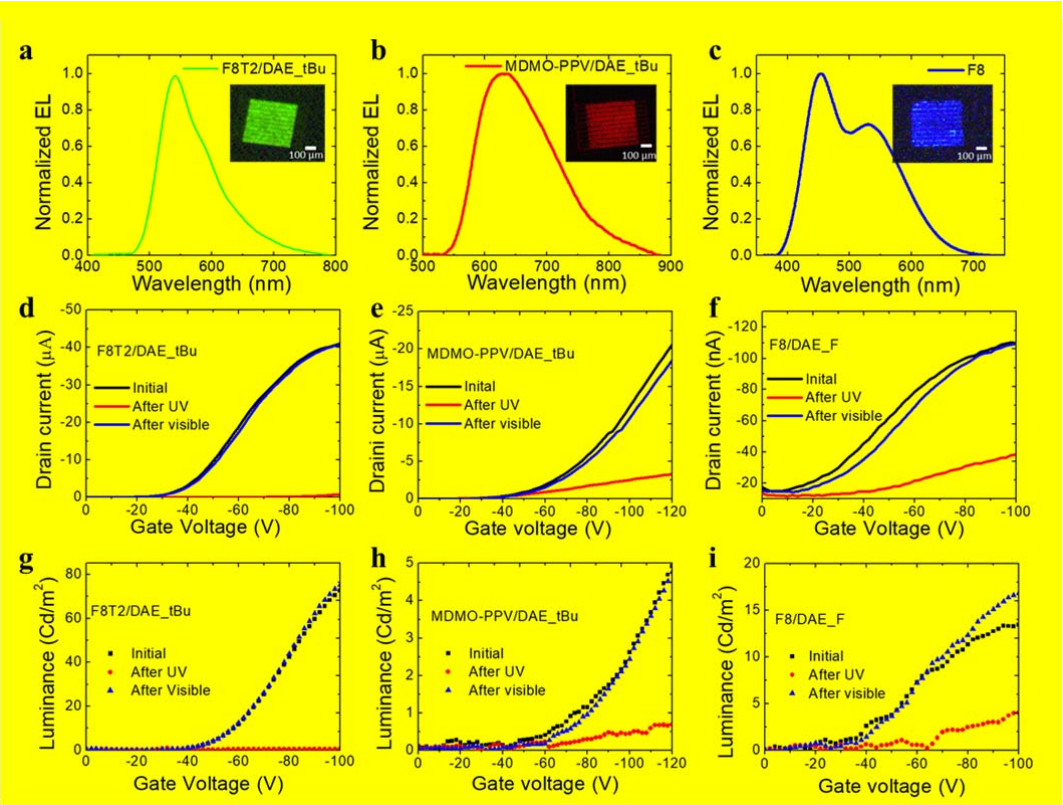

Fig. 2 | EL spectra, optical micrographs, and optoelectronic characteristics. a to **c**, EL spectra and emitting images of F8T2/DAE_tBu, MDMO-PPV/DAE_tBu and F8/DAE_F containing OSOLETs. **d** to **f**, Transfer characteristic curves of F8T2/DAE_tBu OSOLET (V_d = -100 V), MDMO-PPV/DAE_tBu OSOLET (V_d = -120 V) and F8/DAE_F OSOLET (V_d = -100 V), and light-triggered current switching upon UV and visible light irradiation. **g** to **i**, Luminance and light-triggered switching of the luminance in green, red and blue OSOLETs upon UV and visible light irradiation.

The transfer characteristics of green, red, and blue OSOLETs using DAEs as photo-switchable units were measured (Figs. 2d-f). When the DAEs are in their open forms, the hole mobilities extracted from the transfer characteristics in the saturation regime (see supplementary information for device characterization) are about 1.5×10^{-3}, 1×10^{-4}, and 5×10^{-7} $cm^2\ V^{-1}s^{-1}$, respectively. For the sake of comparison, the field-effect mobilities in pristine green, red, and blue polymers based OLETs have been measured to be ca. 5×10^{-3}, 2.0×10^{-4}, and 8×10^{-5} $cm^2\ V^{-1}s^{-1}$, respectively (see

supplementary Fig. S7). Clearly the hole mobility of F8T2 and MDMO-PPV is slightly reduced due to the scattering (and/or residual trapping) of DAEs in the polymeric matrix. However, the mobility in the blue OSOLETs with the open isomer of DAE_F drops by two orders of magnitude with respect to the one using the neat polymer. It appears that domain boundaries and disordered interphase regions in the F8/DAE_F bicomponent film result in a much rougher morphology, thereby hindering charge transport[44].

The luminance of the OSOLETs was collected simultaneously during measurement of the transfer characteristics (Figs. 2g-i), and it shows a similar trend as drain current *vs.* gate voltage (V_g). It should be noted that the pristine F8T2 and MDMO-PPV based OLETs exhibit slightly higher EL intensity as bicomponent ones measured under identical conditions (see supplementary Fig. S7). Interestingly, in the case of F8/DAE_F, despite the reduction of the output current with respect to the pristine material, we observe an increase of luminance, which can be ascribed to the higher PL efficiency (η_{PL}) of F8 in the so-called β-phase as already reported by Perevedentsev and Hsu et al[35,45]. Therefore, F8T2 and MDMO-PPV based OLETs exhibit a minor variation of EQE, between pristine and bicomponent devices (EQE at $V_g = -80$ V for: MDMO-PPV 2×10^{-3} %, MDMO_PPV/DAE_tBu 6×10^{-3} %, F8T2 0.4×10^{-2} %, and F8T2/DAE_tBu 1.0×10^{-2} %). However, the big change in the morphology leads to a remarkable increase of the EQE (again at $V_g = -80$ V) of the F8/DAE_F bicomponent device (1.2 %) when compared to the neat F8 device (1.2

228 $\times 10^{-2}$ %). Although the controlled formation of the β-phase of F8 *via* dipping in
229 solvent/non-solvent mixtures has already been exploited to improve the EQE of
230 F8-based OLEDs[46], no similar investigation has been reported on OLETs yet and we
231 consider this as an additional benefit of combining F8 with DAE_F.
232
233 The remote control *via* light irradiation of the electrical and optical OSOLETs
234 output was investigated. UV (315 nm) irradiation of the OSOLETs yields a
235 remarkable decrease of both drain current and luminance, which we attribute to
236 ring-closing of the DAEs and subsequent efficient trapping of the majority of carriers.
237 In the case of F8T2/DAE_tBu bicomponent devices, the on/off ratios (the ratio of the
238 current/luminance in the initial state and after UV irradiation) in both transport current
239 and EL exceed 500 (see Figs. 2d and 2g). Such a large degree of modulation is
240 comparable with the reports of photo-programmable OLEDs and non-volatile organic
241 memories[47,48]. A high modulation of the drain current and luminance was also
242 observed for MDMO-PPV/DAE_tBu OSOLET devices (85 % decrease in current and
243 87 % decrease in luminance, at $V_g = -120$ V, see Figs. 2e and 2h) as well as
244 F8/DAE_F OSOLET devices (65 % decrease in current and 75 % decrease in
245 luminance, at $V_g = -100$ V, see Figs. 2f and 2i). Further irradiation with green
246 (528 nm) light converts the DAEs back to their open form, and leads to full recovery
247 of the initial state in all three-color OSOLETs. Under the same irradiation conditions,
248 neat polymer based OLETs did not show any modulation of output current and EL
249 (see supplementary Fig. S7).

It should be noted that the energy transfer from the light-emitting polymers to DAEs in their closed form, favored by the spectral overlap of the emission of the polymers with the absorption of the DAEs in ring-closed form, can also contribute to the modulation of the intensity of the emitted light. Indeed, a slight modulation of the PL spectra was detected on the light-emitting polymer/DAE films upon UV and visible irradiation (see supplementary Fig. S9). However, as the switching phenomenon can be observed both on charge transport and light emission, we conclude that energy transfer is not the main operating principle of OSOLETs. Nevertheless, the energy transfer process might help to further modulate the intensity of EL, which can be used to explain the larger modulation degree in the luminance than in the current.

The effect of DAE photoswitching on both output current and luminance of the OSOLETs was monitored over three cycles with alternative UV and visible irradiation (Fig. 3). The large modulation of both maximum drain current and luminance of the three-color OSOLETs, normalized to the initial value for each measurement, is reversible and the optical switching behaviour of OSOLETs is stable over several cycles. Reference OLETs prepared with pristine light-emitting polymers did not show any optically induced modulation, neither on drain current nor on luminance by UV or visible irradiation (see supplementary Fig. S8).

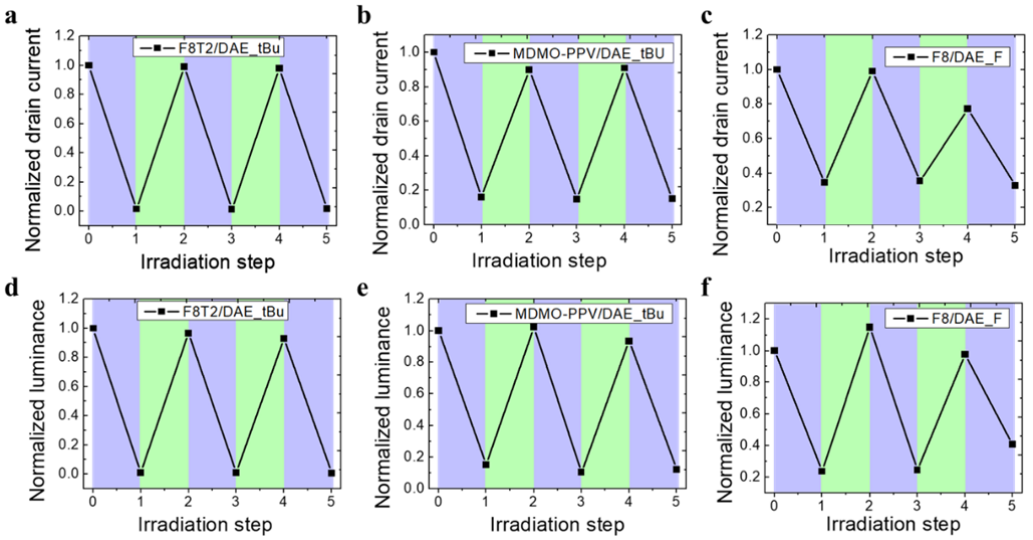

Fig. 3 | Reversible modulation of OSOLETs' current and luminance during irradiation cycles. **a-c** Drain current and **d-f** luminance of green, red, and blue OSOLETs over three irradiation cycles with UV light (315 nm, 0.6 mW, 10 min, violet shaded areas) and visible green light (528 nm, 7 mW, 90 s, green shaded areas). All values are normalized to initial value before any irradiation and the connecting lines serve as 'guides to the eye'.

More importantly, since light is used as an external control of our OSOLETs, it is possible to generate emitting patterns with high spatial and temporal resolution on a single transistor as demonstrated by optical images of patterns created and erased in a single OSOLET (Fig. 4). In the initial configuration, the F8T2/DAE_tBu OSOLET was in an all light-emitting on-state (Fig. 4a). Then, the device was irradiated homogenously using UV light yielding a dark state (Fig. 4b). More interestingly, a well-focused green laser (532 nm) can be used to form patterns on the OSOLET with the aid of a microscope. Fig. 4c shows a light-emitting on-area with a pattern of 'H' shape on the same device. Subsequently, the irradiation of the entire device with green light erased the patterns and the all light-emitting on-state can be seen again (Fig. 4d). The second pattern can be written in the same pixel with another step of UV irradiation and followed by one more laser writing step. Fig. 4f exhibits a pattern

image of an array of dots in the same area, demonstrating the reversible and reproducible patterning of emissive features up to the micron/sub-micron scale. This demonstration using an optimized combination of photoswitch and emissive polymer illustrates the great potential of our approach to reversibly encode high-density visual information in a single display pixel.

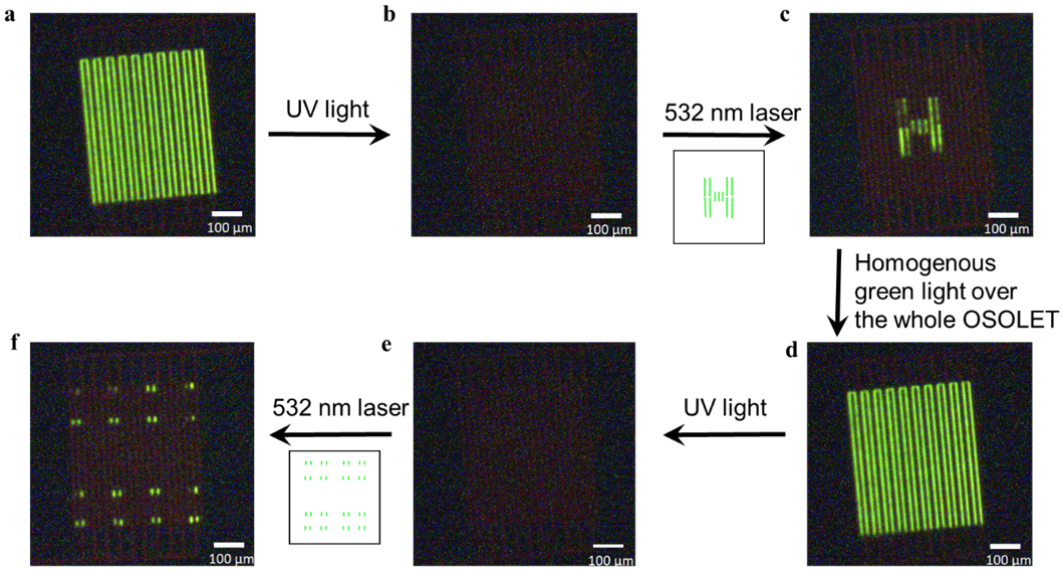

Fig. 4 | Emitting pattern created and erased within a single OSOLET. **a**, Optical image of a F8T2/DAE_tBu OSOLET device biased with $V_d = V_g = -100$ V. **b**, Optical image of a dark state in the same device after UV light irradiation. **c**, Optical image of an 'H' shape emitting pattern from the OSOLET written with a well-focused green laser (532 nm). **d**, Optical image of the second all light-emitting on-state upon homogenous green light irradiation to erase the pattern. **e**, Optical image of the second dark state after homogenous UV irradiation. **f**, Optical image of an array of dots emitting patterns written by the irradiation with a 532 nm laser. The dark area in the pattern is due to the variation of the intensity and/or focus of the laser.

Conclusion

We have fabricated a novel OLET device in which the charge transport and electroluminescence, emitting in the range of the three primary colors, can be switched efficiently and reversibly using light as an external stimulus. The active

312 layer in such optically switchable organic light-emitting transistor (OSOLET)
313 comprises an organic light-emitting semiconductor and a photochromic DAE, in
314 which the photo-tunable energy levels of DAEs can either transport or trap the charge
315 carriers, toggled by UV and visible light irradiation. Such a dual external control is
316 achieved through the engineering of the energy levels of the light-emitting polymers
317 and those of the DAEs isomers. We are able to write and erase emitting patterns in a
318 single OSOLET through a non-invasive and mask-free process, with a spatial
319 resolution of a few micrometers, and a response on the microsecond time scale[22]. The
320 stimuli-responsive multifunctional devices proposed in this work are all readily
321 fabricated *via* solution processing, thus potentially transferrable to roll-to-roll
322 compatible or ink-jet printing lines to produce low-cost and flexible
323 stimuli-responsive (nano)electronics on a large scale. Ink-jet printing appears being a
324 most suitable deposition method to fabricate full color displays by precisely
325 positioning red, green, and blue emissive inks on each sub-pixel.
326
327 In principle, light emission from OLETs in any region of the visible spectrum can be
328 tuned by choosing appropriate photochromic molecules in combination with suitable
329 light-emitting polymers. Future efforts will be directed towards optically switchable
330 OLETs that can be operated at a lower driving power/voltage and yield stronger
331 brightness and a higher ON/OFF ratio. A lowering of the operating voltage and
332 enhancement of the brightness can be achieved *via* the careful selection of (i) the
333 light-emitting materials, which should possess high charge carrier mobility and PL

efficiencies, (ii) the dielectric materials, which should exhibit a high gate capacitance, (iii) the optimal device structures, with a shorter channel length and asymmetric electrodes, and (iv) a hole transport layer and/or an electron transport layer integrated as active component[7,11-16]. Deeper investigations into the amount of incorporated photochromic molecules, energy levels matching, irradiation dose, and the thickness of active film, will surely enable further improvement of the ON/OFF ratios[22,28,47-48]. Our approach opens intriguing perspectives towards the development of novel optically gated, integrated full-color displays, micro-sized light sensors, active optical memories, light controlled inverters, and logic circuitries.

Methods

Methods, including statements of data availability and any associated accession codes and references, are available in the online version of the paper.

References

1 Muccini, M. A bright future for organic field-effect transistors. *Nature Mater.* **5**, 605–613 (2006).

2 Cicoira, F. & Santato, C. Organic Light Emitting Field Effect Transistors: Advances and Perspectives. *Adv. Funct. Mater.* **17**, 3421-3434 (2007).

3 Santato, C., Cicoira, F. & Martel, R. Spotlight on organic transistors. *Nature Photon.* **5**, 392–393 (2011).

4 Zhang, C., Chen, P. & Hu, W. Organic light-emitting transistors: materials, device configurations, and operations. *Small* **12**, 1252-1294 (2016).

5 Zaumseil, J. & Sirringhaus, H. Electron and ambipolar transport in organic field-effect transistors. *Chem. Rev.* **107**, 1296-1323 (2007).

6 Zaumseil, J., Friend, R. H. & Sirringhaus, H. Spatial control of the recombination zone in an ambipolar light-emitting organic transistor. *Nature Mater.* **5**, 69–74 (2005).

7 Hsu, B. B. Y. *et al.* Control of efficiency, brightness, and recombination zone in light-emitting field effect transistors. *Adv. Mater.* **24**, 1171-1175 (2012).

8 Swensen, J. S., Soci, C. & Heeger, A. J. Light emission from an ambipolar semiconducting polymer field-effect transistor. *Appl. Phys. Lett.* **87**, 253511 (2005).

9 Bisri, S. Z. *et al.* High mobility and luminescent efficiency in organic single-crystal light-emitting transistors. *Adv. Funct. Mater.* **19**, 1728–1735 (2009).

10 Capelli, R. *et al.* Interface functionalities in multilayer stack organic light emitting transistors (OLETs). *Adv. Funct. Mater.* **24**, 5603-5613 (2014).

11 Capelli, R. *et al.* Organic light-emitting transistors with an efficiency that outperforms the equivalent light-emitting diodes. *Nature Mater.* **9**, 496–503 (2010).

12 McCarthy, M. A. *et al.* Low-voltage, low-power, organic light-emitting transistors for active matrix displays. *Science* **332**, 570–573 (2011).

13 Zaumseil, J., Donley, C. L., Kim, J. S., Friend, R. H. & Sirringhaus, H. Efficient top-gate, ambipolar, light-emitting field-effect transistors based on a green-light-emitting polyfluorene. *Adv. Mater.* **18**, 2708–2712 (2006).

14 Gwinner, M. C. *et al.* Highly efficient single-layer polymer ambipolar light-emitting field-effect transistors. *Adv. Mater.* **24**, 2728–2734 (2012).

15 Ullah, M. *et al.* Simultaneous enhancement of brightness, efficiency, and switching in RGB organic light emitting transistors. *Adv. Mater.* **25**, 6213–6218 (2013).

16 Park, S. K. *et al.* Highly luminescent 2D-type slab crystals based on a molecular charge-transfer complex as promising organic light-emitting transistor materials. *Adv. Mater.* **29**, 1701346 (2017).

17 Yang, Y., da Costa, R. C., Fuchter, M. J. & Campbell, A. J. Circularly polarized light detection by a chiral organic semiconductor transistor. *Nature Photon.* **7**, 634–638 (2013).

18 Kim, Y. L. *et al.* Voltage-switchable photocurrents in single-walled carbon nanotube–silicon junctions for analog and digital optoelectronics. *Nature Photon.* **8**, 239–243 (2014).

19 Zhang, Y. J., Oka, T., Suzuki, R., Ye, J. T. & Iwasa, Y. Electrically switchable chiral light-emitting transistor. *Science* **344**, 725–728 (2014).

20 Wang, X. *et al.* A spectrally tunable all-graphene-based flexible field-effect light-emitting device. *Nature Commun.* **6**, 7767 (2015).

21 Zhang, X. Y., Hou, L. L. & Samorì, P. Coupling carbon nanomaterials with photochromic molecules for the generation of optically responsive materials. *Nature Commun.* **7**, 11128 (2016).

22 Orgiu, E. *et al.* Optically switchable transistor via energy-level phototuning in a bicomponent organic semiconductor. *Nature Chem.* **4**, 675–679 (2012).

23 Gemayel, M. E. *et al.* Optically switchable transistors by simple incorporation of photochromic systems into small-molecule semiconducting matrices. *Nature Commun.* **6**, 6330 (2015).

24 Borjesson, K. *et al.* Optically switchable transistors comprising a hybrid photochromic molecule/n-type organic active layer. *J. Mater. Chem. C* **3**, 4156–4161 (2015).

25 Irie, M. & Mohri, M. Thermally irreversible photochromic systems. Reversible photocyclization of diarylethene derivatives. *J. Org. Chem.* **53**, 803–808 (1988).

26 Irie, M., Fukaminato, T., Matsuda, K. & Kobatake, S. Photochromism of diarylethene molecules and crystals: memories, switches, and actuators. *Chem. Rev.* **114**, 12174–12277 (2014).

27 Hou, L., Zhang, X., Pijper, T. C., Browne, W. R. & Feringa, B. L. Reversible photochemical control of singlet oxygen generation using diarylethene photochromic switches. *J. Am. Chem. Soc.* **136**, 910–913 (2014).

28 Leydecker, T. *et al.* Flexible non-volatile optical memory thin-film transistor device with over 256 distinct levels based on an organic bicomponent blend. *Nature Nanotech.* **11**, 769–775 (2016).

29 Herder, M. *et al.* Improving the fatigue resistance of diarylethene switches. *J. Am. Chem. Soc.*

137, 2738–2747 (2015).

30 Herder, M. *et al.* Light-controlled reversible modulation of frontier molecular orbital energy levels in trifluoromethylated diarylethenes. *Chem. Eur. J.* **23**, 3743–3754 (2017).

31 Salleo, A., Chabinyc, M. L., Yang, M. S. & Street, R. A. Polymer thin-film transistors with chemically modified dielectric interfaces. *Appl. Phys. Lett.* **81**, 4383–4385 (2002).

32 Ito, Y. *et al.* Crystalline ultrasmooth self-assembled monolayers of alkylsilanes for organic field-effect transistors. *J. Am. Chem. Soc.* **131**, 9396–9404 (2009).

33 Lee, T.-W. & Park, O. O. The effect of different heat treatments on the luminescence efficiency of polymer light-emitting diodes. *Adv. Mater.* **12**, 801-804 (2000).

34 Grell, M., Bradley, D. D. C., Inbasekaran, M. & Woo, E. P. A glass-forming conjugated main-chain liquid crystal polymer for polarized electroluminescence applications. *Adv. Mater.* **9**, 798–802 (1997).

35 Perevedentsev, A., Chander, N., Kim, J. S. & Bradley, D. D. C. Spectroscopic properties of poly(9,9-dioctylfluorene) thin films possessing varied fractions of β-phase chain segments: enhanced photoluminescence efficiency via conformation structuring. *J. Polym. Sci. Pol. Phys.* **54**, 1995–2006 (2016).

36 Caruso, M. E., Lattante, S., Cingolani, R. & Anni, M. Microscopic investigation of the poly(9,9-dioctylfluorene) photoluminescence dependence on the deposition conditions by confocal laser microscopy. *Appl. Phys. Lett.* **88**, 181906 (2006).

37 Lim, S. F. *et al.* Suppression of green emission in a new class of blue-emitting PF copolymers with twisted biphenyl moieties. *Adv. Funct. Mater.* **15**, 981–988 (2005).

38 List, E. J. W., Guentner, R., Scanducci de Freitas, P. & Scherf, U. The effect of keto defect sites on the emission properties of polyfluorene-type materials. *Adv. Mater.* **14**, 374-378 (2002).

39 Honmou, Y. *et al.* Single-molecule electroluminescence and photoluminescence of polyfluorene unveils the photophysics behind the green emission band. *Nature Commun.* **5**, 4666 (2014).

40 Gong, X. *et al.* Stabilized blue emission from polyfluorene-based light-emitting diodes: elimination of fluorenone defects. *Adv. Funct. Mater.* **13**, 325-330 (2003).

41 Hepp, A. *et al.* Light-emitting field-effect transistor based on a tetracene thin film. *Phys. Rev. Lett.* **91**, 157406 (2003).

42 Santato, C. *et al.* Tetracene-based organic light-emitting transistors: optoelectronic properties and electron injection mechanism. *Synth. Met.* **146**, 329–334 (2004).

43 Roelofs, W. S. C., Adriaans, W. H., Janssen, R. A. J., Kemerink, M. & Leeuw, D. M. d. Light emission in the unipolar regime of ambipolar organic field-effect transistors. *Adv. Funct. Mater.* **23**, 4133–4139 (2013).

44 Redecker, M., Bradley, D. D. C., Inbasekaran, M. & Woo, E. P. Mobility enhancement through homogeneous nematic alignment of a liquid-crystalline polyfluorene. *Appl. Phys. Lett.* **74**, 1400–1402 (1999).

45 Hsu, B. B. Y. *et al.* Ordered polymer nanofibers enhance output brightness in bilayer light-emitting field-effect transistors. *ACS Nano* **7**, 2344–2351 (2013).

46 Lu, H. H., Liu, C. Y., Chang, C. H. & Chen, S. A. Self-dopant formation in poly(9,9-di-n-octylfluorene) via a dipping method for efficient and stable pure-blue electroluminescence. *Adv. Mater.* **19**, 2574–2579 (2007).

47 Zacharias, P., Gather, M. C., Köhnen, A., Rehmann, N. & Meerholz, K. Photoprogrammable organic light-emitting diodes. *Angew. Chem. Int. Ed.* **48**, 4038–4041 (2009).

48 Scott, J. C. & Bozano, L. D. Nonvolatile memory elements based on organic materials. *Adv. Mater.* **19**, 1452–1463 (2007).

Acknowledgement

We acknowledge funding from the European Commission through the Marie Sklodowska-Curie ITN project iSwitch (GA-642196), the Marie Sklodowska-Curie ITN project SYNCHRONICS (GA-643238), the ERC projects SUPRAFUNCTION (GA-257305) and LIGHT4FUNCTION (GA-308117), the Agence Nationale de la Recherche through the Labex project CSC (ANR-10-LABX-0026 CSC) within the Investissement d'Avenir program (ANR-10-120 IDEX-0002-02), and the International Center for Frontier Research in Chemistry (icFRC) as well as the German Research Foundation (via SFB 765 and SFB 951). FC is a Royal Society Wolfson Research Merit Award holder.

Author contributions

L.H., X.Z., and P.S. conceived the experiments. M.H., B.M.S., M.P., and S.H. synthesized the DAEs. L.H. did UV/visible absorption and PL measurements, and X.Z. performed AFM (the F8/DAE_tBu sample by G.C.) and CV measurements. L.H. and X.Z. designed the devices, performed the electrical experiments and carried out emitting patterns writings. G.F.C., G.C., and F.C designed and built the device characterization setup. G.F.C., G.C., and L.H. performed the quantitative OLET device characterization. All authors discussed the results and contributed to the interpretation of data. L.H., X.Z., and P.S. co-wrote the paper with inputs from all co-authors.

Competing interests

The authors declare no competing financial interests

Additional information

Supplementary information is available in the online version of the paper. Reprints and permissions information is available online at www.nature.com/reprints. Correspondence and requests for materials should be addressed to P.S.

Supplementary Information

Optically switchable organic light-emitting transistors

Lili Hou[1], Xiaoyan Zhang[1,4], Giovanni F. Cotella[2], Giuseppe Carnicella[2], Martin Herder[3], Bernd M. Schmidt[3], Michael Pätzel[3], Stefan Hecht[3,*], Franco Cacialli[2,*], Paolo Samorì[1,*]

1 Université de Strasbourg, CNRS, ISIS, 8 alleé Gaspard Monge, 67000 Strasbourg, France. Email: samori@unistra.fr

2 Department of Physics and Astronomy (CMMP Group) and London Centre for Nanotechnology, University College London, Gower Street, London WC1E 6BT, United Kingdom. Email: f.cacialli@ucl.ac.uk

3 Department of Chemistry & IRIS Adlershof, Humboldt-Universität zu Berlin, Brook-Taylor-Straße 2, 12489 Berlin, Germany. Email: sh@chemie.hu-berlin.de

4 Present address: Department of Chemistry and Chemical Engineering, Chalmers University of Technology, 412 96 Gothenburg, Sweden.

Table of Contents

1. Materials and characterization

Butyl acetate (Sigma-Aldrich, ≥99%, anhydrous), *p*-xylene (Sigma-Aldrich, ≥99%, anhydrous), and ethyl acetate (Sigma-Aldrich, 99.8%, anhydrous) were used without any further purification. Poly[2-methoxy-5-(3′,7′-dimethyloctyloxy)-1,4-phenylenevinylene] (MDMO-PPV, Sigma-Aldrich), poly(9,9-di-*n*-octylfluorenyl-2,7-diyl) (F8, Sigma-Aldrich), and poly(9,9-dioctylfluorene-*alt*-bithiophene) (F8T2, Ossila) were used as received. The detailed synthesis, photochemistry in solution and energy level determination of DAE_tBu and DAE_F was previously reported[1–3]. UV/visible absorption spectra were recorded on a JASCO 650 spectrometer under ambient conditions. Photoluminescence spectra were measured on a Cary Eclipse fluorescence spectrophotometer under ambient conditions. AFM images were recorded using a Nanoscope (Veeco Multimode V) in tapping mode at ambient conditions.

Cyclic voltammetry (CV) was carried out on a PGSTAT204 instrument (Autolab). A three-electrode configuration was used, consisting of a platinum disc as the working electrode (2 mm diameter), a platinum wire as the counter electrode and a silver/silver chloride electrode as the reference electrode. Samples for CV measurement were prepared by drop-casting the respective polymer solution in chloroform onto the working electrode. The measurement was performed in 0.1 M Bu_4NPF_6 dissolved in acetonitrile. Ferrocene was used as an external standard. Onset oxidation potential is used to calculate the HOMO level of polymers, based on the equation $E^{HOMO} = -e \cdot E_{oxvsFc/Fc+} - 4.8$ eV used by Pommerehne et al[4].

The irradiation on the OLETs was carried out inside the glove-box, a UV LED (Thorlabs LED315W, 0.6 mW, 315 nm, FWHM = 10 nm) and a green LED (Thorlabs LED528EHP, 7 mW, 528 nm, FWHM = 35 nm) were used. In general, the PSS was reached under UV irradiation for 10 mins and recovery within 90 s under visible light. For UV/visible absorption and PL spectroscopies, UV light irradiation was carried out using an analysis lamp (312 nm, 6 W, Herolab) for 20 s, and visible light irradiation was performed using a white lamp (Dolan-Jenner MI-150 Illuminator) coupled with a long pass filter (> 520 nm) for 30 s. The patterned images of the OLETs were created by using a focused laser (focus ca. 2 μm^2, 532 nm, 60 mW cm^{-2}), and the writing process was controlled under a microscope with a 50× objective on a Renishaw 1000 Raman setup.

2. Device fabrication

Devices were fabricated on the substrates of n^{++} Si as bottom gate and 230 nm of thermally grown SiO_2 as the gate dielectric (IPMS Fraunhofer Institute). Interdigitated gold source and drain electrodes are prepatterned with a channel width of 1 cm and a length of 2.5 µm. The substrates were cleaned by ultrasonication in acetone and isopropanol for 20 min, blow dried with a nitrogen flow, and then treated by ozone for 5 min (Novascan, Digital UV Ozone system) followed by 25 min incubation in dark before transferring the device into a glove box. A self-assembled monolayer of OTS (Sigma-Aldrich, ≥ 90%) was chemisorbed on SiO_2/Si substrates by immersion of the substrates in a 10 mM OTS in toluene at 60 °C for 2 h before they were left at room temperature overnight in the glove box, and washed with toluene and isopropanol.

The green emitting layer was spun from a 10 mg/mL solution of F8T2 in anhydrous *p*-xylene, and the thickness was ≈ 80 nm. The device was annealed at 170 □ for 20 min. DAE_tBu was dissolved in anhydrous *n*-butyl acetate at a concentration of 1 mg/mL, and spun on top of the F8T2 film. Subsequent annealing at 80 □ for 1 h was applied to allow the diffusion of DAE molecules into F8T2 matrix.

The red emitting layer was spun from an 8 mg/ml solution of MDMO-PPV in anhydrous *p*-xylene, and the thickness was ≈ 80 nm. The device was annealed at 170 □ for 20 min. DAE_tBu was dissolved in anhydrous *n*-butyl acetate at a concentration of 1 mg/mL, and spun on top of the MDMO-PPV film. Subsequent annealing was applied at 80 □ for 1 h to allow the diffusion of DAE molecules into MDMO-PPV matrix.

The blue emitting layer was spun from a 20 mg/mL solution of F8 in anhydrous *p*-xylene, and the thickness was ≈ 100 nm. The device was briefly annealed at 170 □ for 2 min. DAE_F was dissolved in anhydrous ethyl acetate with the concentration of 2 mg/mL, and spun on top of the F8 film. Subsequent annealing at 40 □ for 1.5 h was applied to allow the diffusion of DAE molecules into F8 matrix.

The neat light-emitting polymers based OLETs were prepared using the same method as described above without deposition of DAEs.

3. Device characterization

Devices were characterized in a dry and nitrogen-filled Mbraun glove-box. Electrical characteristics of OLETs were collected through the PM5 Cascade Microtech probe station connected with a Keithley semiconductor analyzer 4200-scs. OSOLETs transfer characteristics was collected by scanning the gate voltage from 0 V to -100 V or 0 V to -120 V, with the drain voltage set at -100 V or -120 V. The light output of devices was calculated from the photocurrent signal of a calibrated silicon photodiode, amplified by the Eg&G Instruments 5182 preamplifier. The area of the photodiode was 15 mm^2, the distance between device and photodiode amounted to 5.2 mm, and the area of device emission was 0.025 mm^2. Electrical and optical characteristics were collected simultaneously. Device irradiation was performed in glovebox *via* LEDs connected to a remotely controllable microprocessor. The EL spectra of emitting devices were collected by connecting an optical fibre through a feedthrough in the glove-box to an ANDOR-Shamrock 163 spectrometer coupled to an ANDOR-Newton charge-coupled device (CCD) unit held outside the glove-box. The EL images were recorded on a microscope (Leica S6D) with a charge coupled device (CCD) colour camera.

The following equation is used to calculate the mobility (μ_{sat}) of our devices.

$$\mu_{sat} = \frac{2\left[\frac{\partial\sqrt{I_d^{sat}}}{\partial V_g}\right]^2}{C_i\frac{W}{L}}$$

Where C_i is the capacitance of the dielectric (1.5×10^{-8} F cm^{-2}), W is the width of the channel, L is the length of the channel, V_g is the gate voltage.

4. UV/visible absorption and photoluminescence (PL) spectra of light-emitting polymers

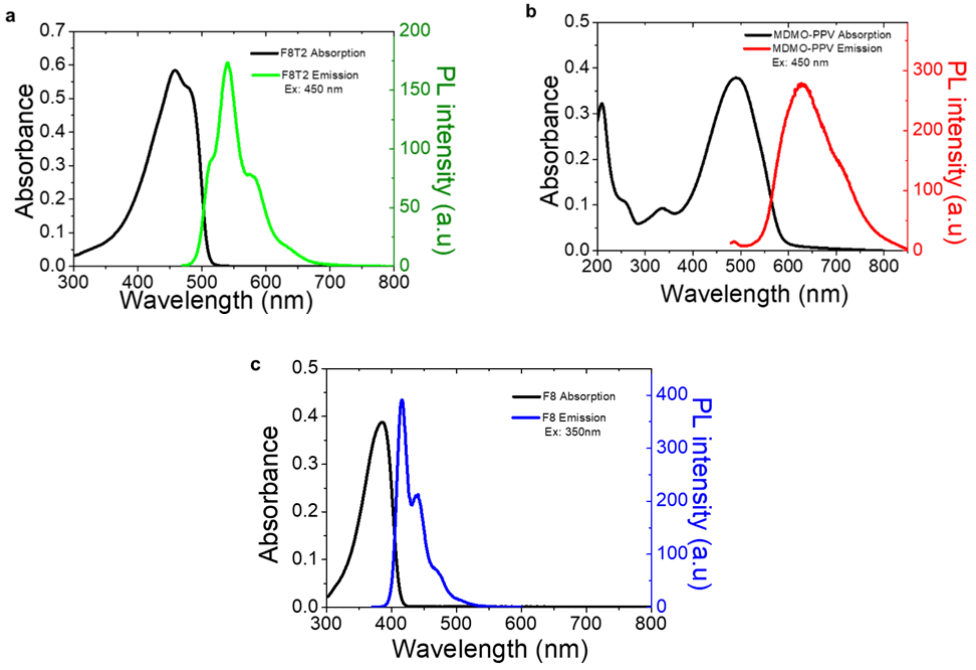

Fig. S1. UV/visible absorption and PL spectra of a film of **a**, F8T2, **b**, MDMO-PPV, and **c,** F8. The films of neat light-emitting polymers were prepared on quartz substrates using the same conditions and procedures as OSOLETs but without incorporation of DAEs.

5. Cyclic voltammetry (CV) measurement of light-emitting polymers

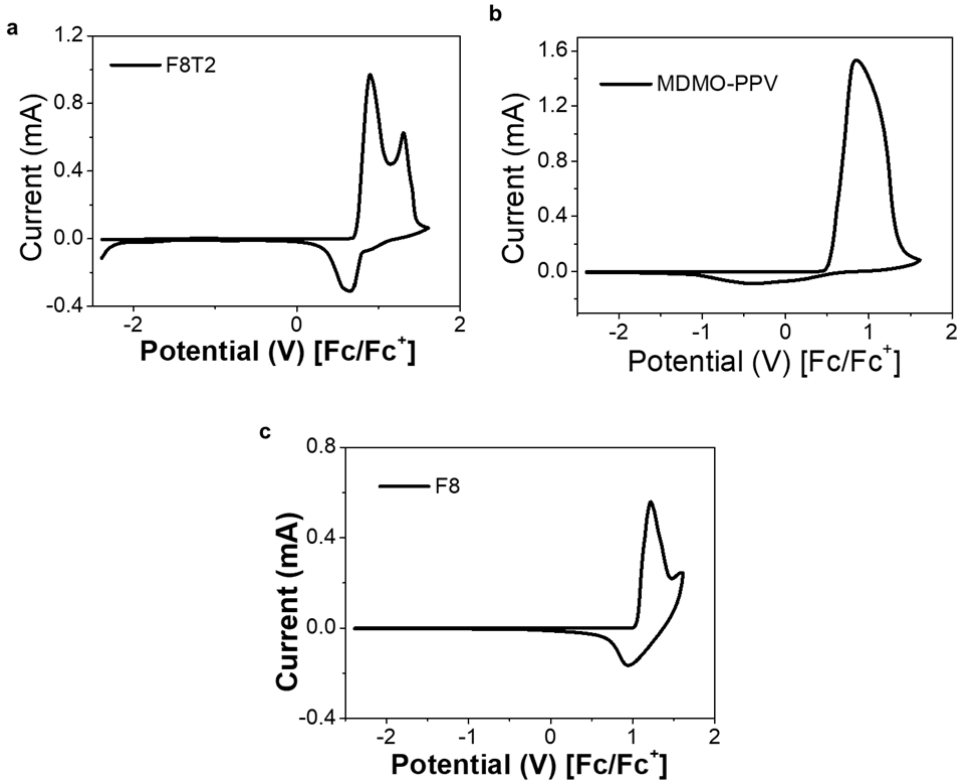

Fig. S2. CV curves of **a**, F8T2, **b**, MDMO-PPV, and **c**, F8 on a platinum disc measured in acetonitrile containing 0.1 M Bu_4NPF_6 at 25 °C at a scan rate of 0.03 V/s, using a three-electrode configuration.

6. Atomic force microscopy (AFM) images of neat light-emitting polymers and light emitting polymer/DAE films

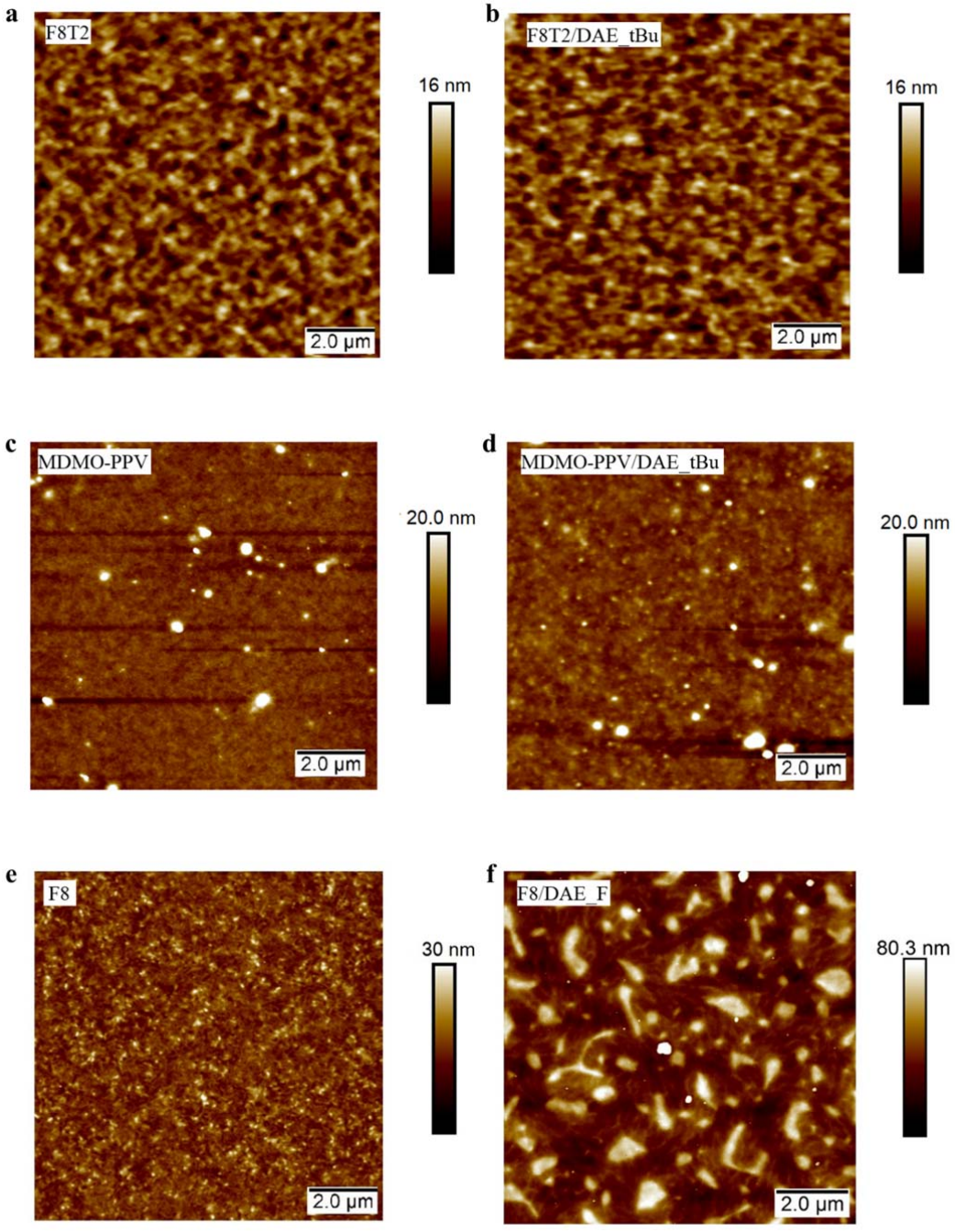

Fig. S3. AFM images of the film of **a**, neat F8T2, **b**, F8T2/DAE_tBu, **c**, neat MDMO-PPV, **d**, MDMO-PPV/DAE_tBu, **e**, neat F8, and **f**, F8/DAE_F.

7. UV/visible absorption spectra and photochemical switching of neat DAE films

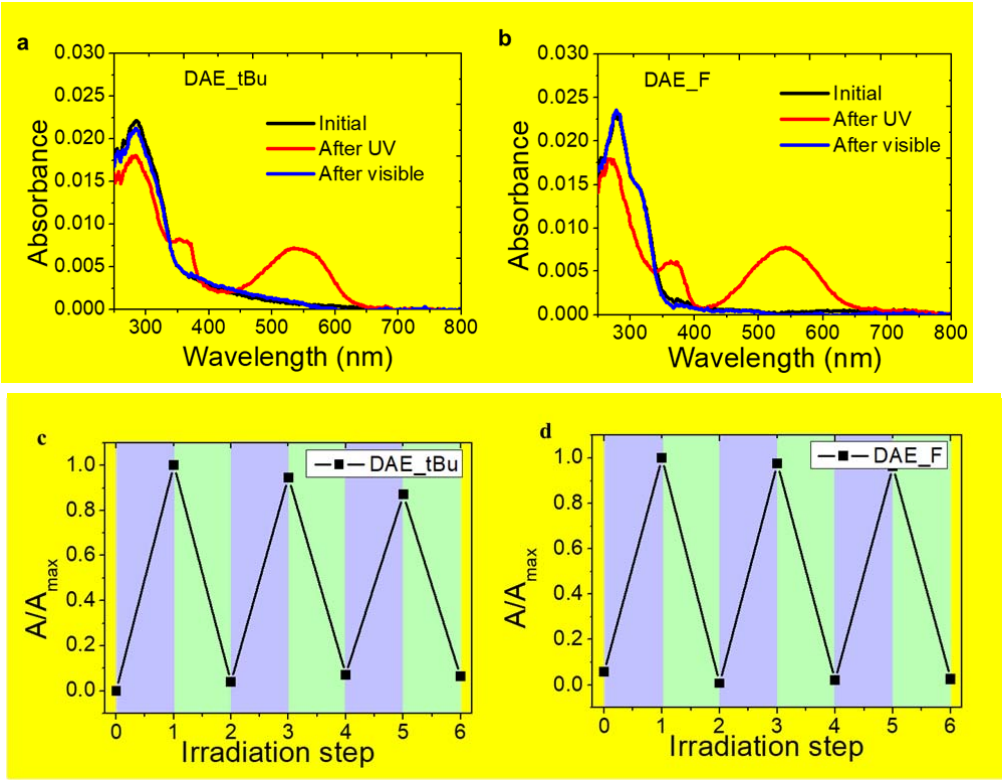

Fig. S4. UV/visible absorption spectra of the films of **a**, DAE_tBu, and **b**, DAE_F after UV (312 nm) and visible irradiation (> 520 nm). Photochemical switching of **c**, DAE_tBu, and **d**, DAE_F in the solid state over three irradiation cycles with UV light (violet shaded areas) and visible green light (green shaded areas). The absorbance at λ_{abs} = 530 nm is normalized to the maximum absorbance after the first UV irradiation step. DAEs were spin-coated on quartz substrates by a solution of DAE_tBu (1 mg/mL in anhydrous *n*-butyl acetate) and DAE_F 2 mg/mL in anhydrous ethyl acetate), respectively.

8. UV/visible absorption spectra of light-emitting polymer/DAE films

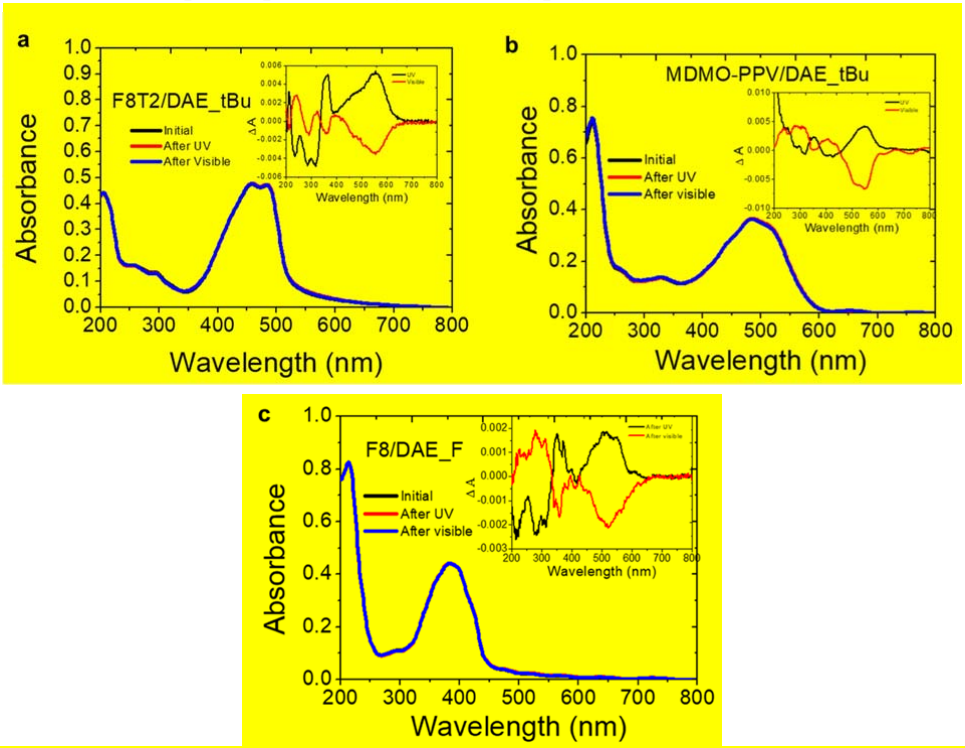

Fig. S5. UV/visible absorption spectra of the films of **a**, F8T2/DAE_tBu, **b**, MDMO-PPV/DAE_tBu, **c**, F8/DAE_F8, and the spectra after UV and visible irradiation. The differential changes in absorbance after irradiation are plotted in the inset figures with the subtraction from last spectrum, i.e., the spectrum after UV light irradiation subtracting the initial one, and the spectrum after visible light irradiation subtracting the one after UV light irradiation. The bicomponent films of light-emitting polymer/DAE were prepared on quartz substrates using the same condition and procedure as the fabrication of OSOLETs.

By determining the absorption coefficient (see Table S1), the density of each light-emitting polymer film was calculated from the absorbance in Fig. S5. As the open DAEs are transparent in the visible region, the density of the closed DAEs could be estimated from the differential changes in absorbance upon UV irradiation. By assuming the same photostationary state (PSS) in thin film as in solution, the doping concentration of the initial open DAE was quantified being 2.0 wt% in F8T2, 4.7 wt% in MDMO-PPV and 2.5 wt% in F8.

Table S1. Spectroscopic properties of DAEs and light-emitting polymers

	Absorption coefficient (α / L g^{-1} cm^{-1})	Photostationary state (PSS)
DAE_tBu closed	32 (523 nm)	90 %
DAE_F closed	20 (512 nm)	96 %
F8T2	93 (485 nm)	-
MDMO-PPV	75 (490 nm)	-
F8	102 (385 nm)	-

9. LUMO levels of light-emitting polymers and DAEs

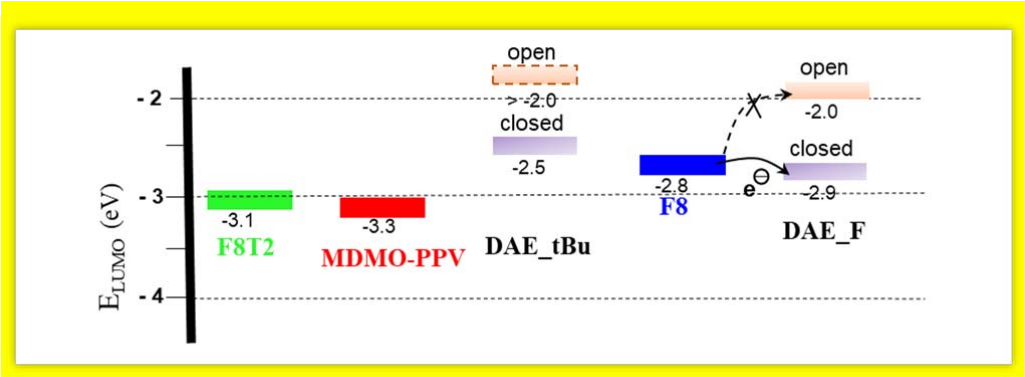

Scheme. S1. LUMO levels of light-emitting polymers and DAEs in their open (orange) and closed (purple) form[3]. The values of light-emitting polymers were calculated from $E^{LUMO} = E^{HOMO} + Eg^{Opt}$, where Eg^{Opt} was determined based on the UV absorption spectra of light emitting polymers (Fig. S1), in line with previously reports[5-7].

The LUMO levels of DAE_tBu both in its open and closed form are higher in energy than the LUMO levels of F8T2 and MDMO-PPV, and there is no driving force for electron transfer from green and red polymer to either photoisomer of DAE_tBu[8]. Because of these reasons, the light irradiation would not result in any photomodulation in electron transport. The difference in the LUMO levels of DAE_F in the closed form and F8 amounts to 0.1 eV, which could in principle result in shallow trapping for electrons upon UV irradiation. However, since F8 is a very good hole transporting material and exhibits poor electron transport characteristics, we are not able to observe the presence of electron transport and light modulation thereof in our F8 based OLET.

10. Optical micrographs of F8T2 OLET

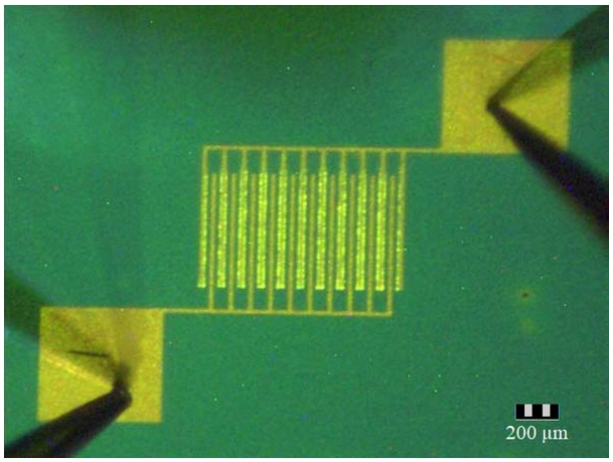

Fig. S6. Optical micrographs of F8T2 OLET (L = 20 µm, W = 1 cm) and its emission zone at $V_g = -100$ V and $V_d = -100$ V.

11. Transfer curve and EL of neat light-emitting polymers based OLETs

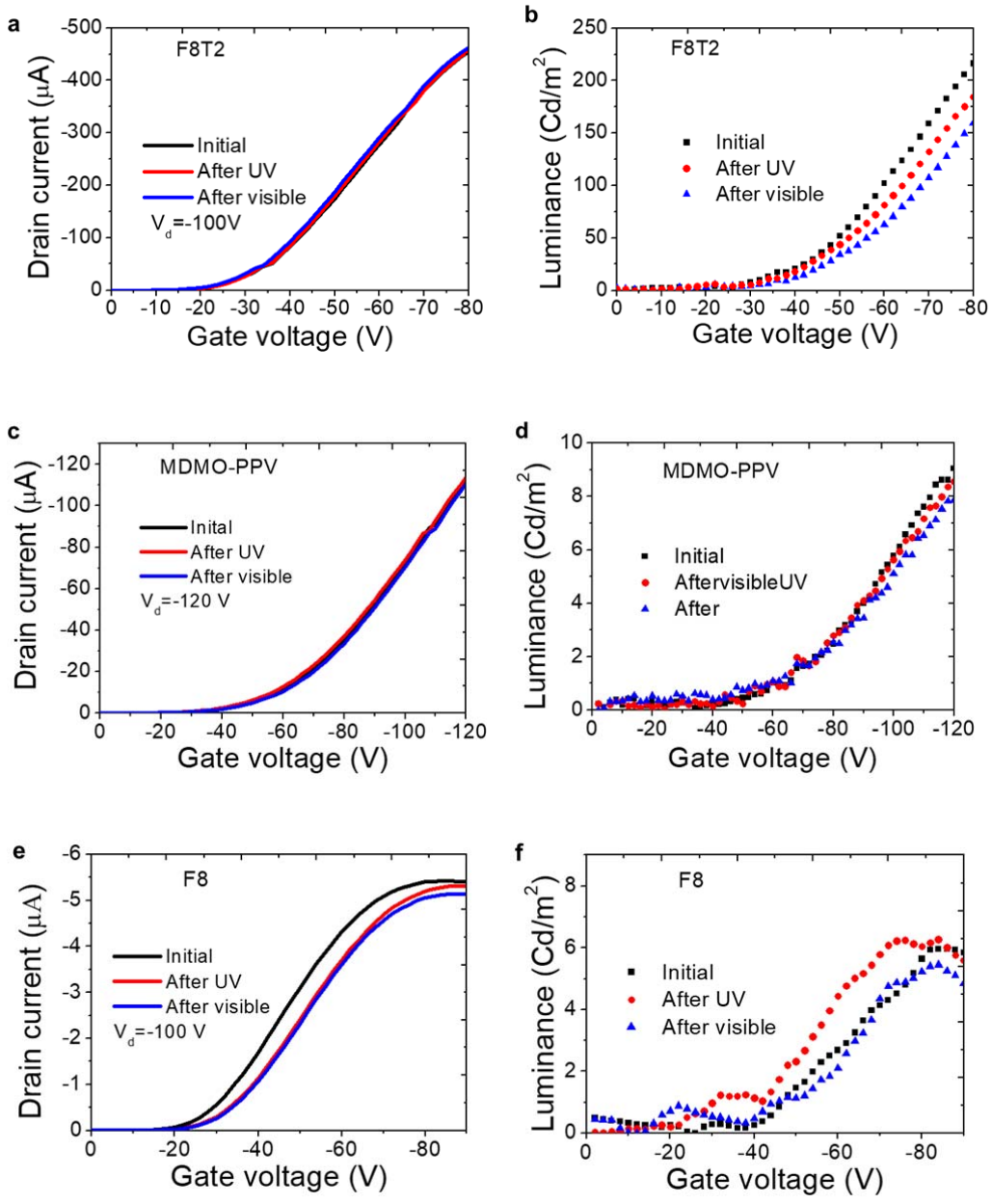

Fig. S7. The transfer characteristic curves and luminance of **a**, **b**, neat F8T2 OLET at drain voltage −100 V, **c**, **d**, MDMO-PPV OLET at drain voltage −120 V, and **e**, **f**, F8 OLET at drain voltage −100 V, and their optical switching upon UV and visible light irradiation.

12. Reversibility of neat light-emitting polymers based OLETs

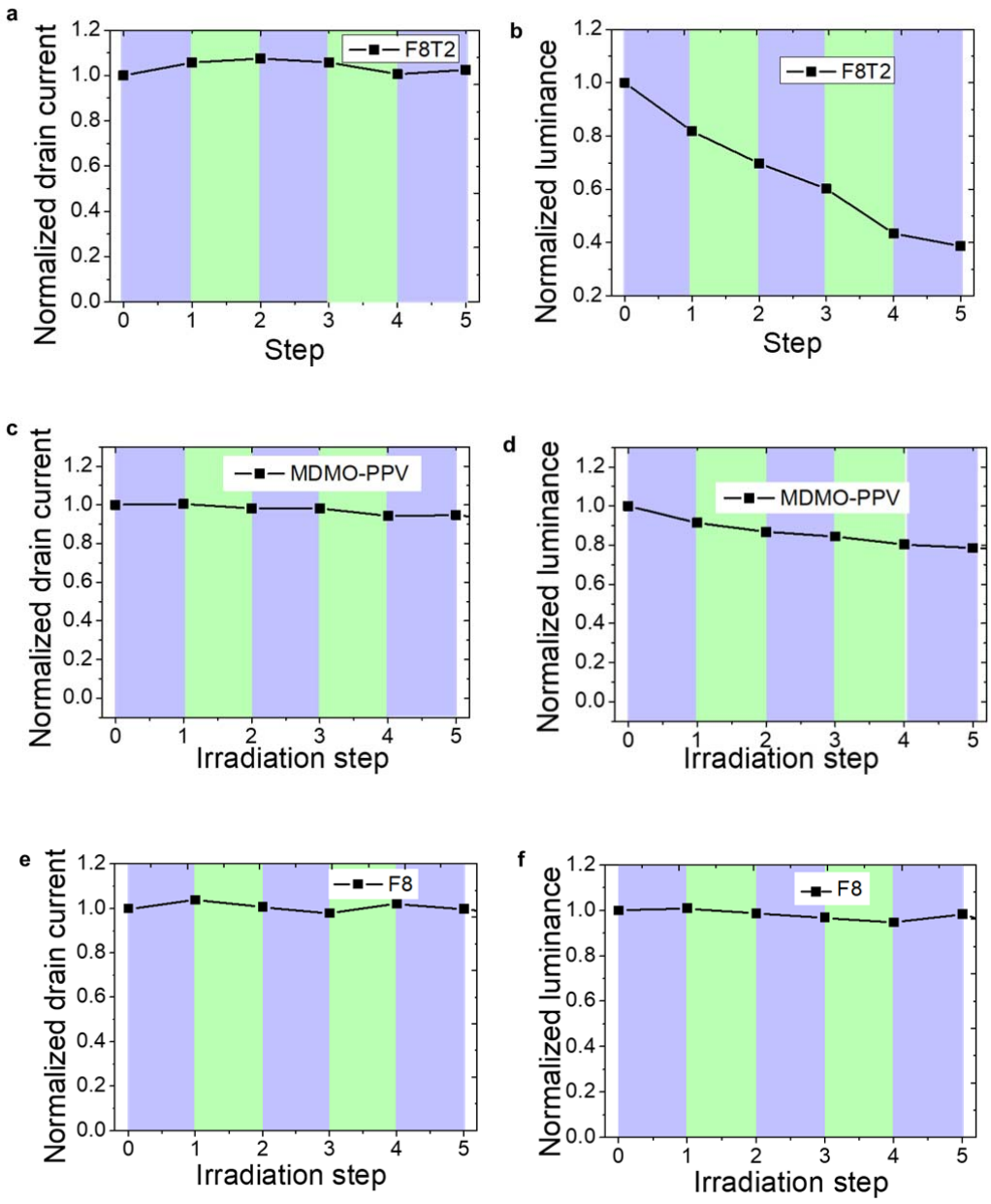

Fig. S8. Photo switching of transistor characteristics and optoelectronic characteristics of **a**, **b**, neat F8T2, **c**, **d**, MDMO-PPV and **e**, **f**, F8 based OLETs over three irradiation cycles. The reduction in luminance of F8T2 with the light irradiation was due to the high drain current of the pure F8T2 OLET[9-11].

13. PL spectra of light-emitting polymer/DAE bicomponent films under light irradiation.

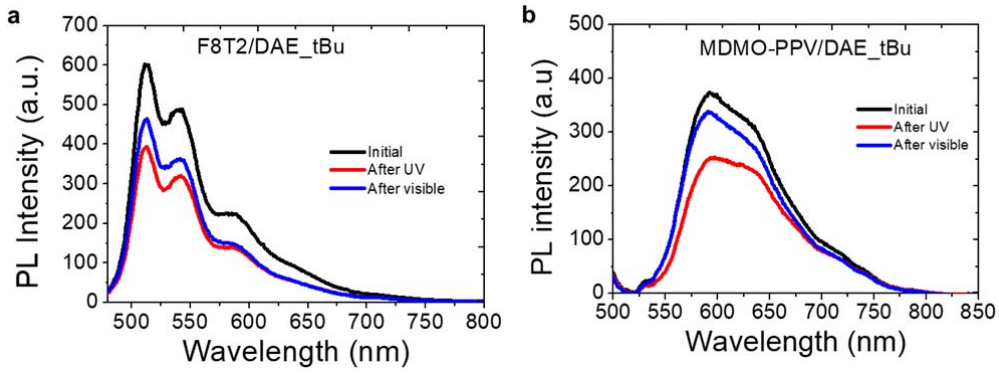

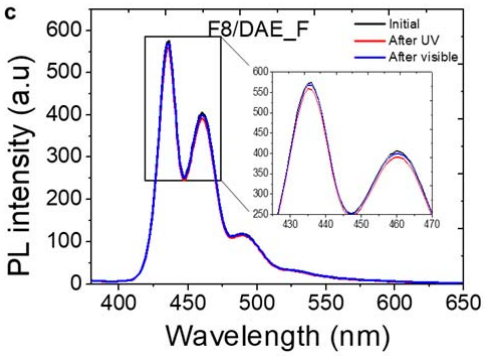

Fig. S9. PL spectra of the films of **a**, F8T2/ DAE_tBu, **b**, MDMO-PPV/DAE_tBu, **c**, F8/DAE_F, and their response after UV and visible light irradiation. The films of light-emitting polymer/DAE were prepared on quartz substrates using the same condition and procedure as the fabrication of OSOLETs.

Decrease in PL intensity of F8T2/DAE_tBu, MDMO-PPV/DAE_tBu and F8/DAE_F films were observed after UV irradiation. The ratio of PL intensity at the highest emissive peak between before and after UV irradiation was ca. 1/0.63, 1/0.68 and 1/0.97, respectively, which is consistent with the area of spectral overlap between absorption spectra of the closed form of DAEs and the PL spectra of the emitting polymers. Further irradiation with visible light, resulting an increase of PL intensity. The non-complete recovery of PL intensity can be explained by the degradation of the emitting polymers under ambient conditions, especially in the case of F8T2 and MDMO-PPV.

14. References

1. Gemayel, M. E. *et al.* Optically switchable transistors by simple incorporation of photochromic systems into small-molecule semiconducting matrices. *Nature Commun.* **6**, 6330 (2015).

2. Herder, M. *et al.* Improving the fatigue resistance of diarylethene switches. *J. Am. Chem. Soc.* **137**, 2738–2747 (2015).

3. Herder, M. *et al.* Light-controlled reversible modulation of frontier molecular orbital energy levels in trifluoromethylated diarylethenes. *Chem. Eur. J.* **23**, 3743–3754 (2017).

4. Pommerehne, J. *et al.* Efficient two layer leds on a polymer blend basis. *Adv. Mater.* **7**, 551–554 (1995).

5. Sirringhaus H. et al. Mobility enhancement in conjugated polymer field-effect transistors through chain alignment in a liquid-crystalline phase. *Appl. Phys. Lett.* **77**, 406-408 (2000).

6. Morgado J. Improved efficiency of light-emitting diodes based on polyfluorene blends upon insertion of a poly(p-phenylene vinylene) electron- confinement layer. *Appl. Phys. Lett.* **80**, 2436 (2002)

7. Beek W. J. E., Wienk M. M. & Janssen R. A. J. Efficient hybrid solar cells from zinc oxide nanoparticles and a conjugated polymer. *Adv. Mater.* **16**, 1009-1013 (2004)

8. Borjesson, K. *et al*. Optically switchable transistors comprising a hybrid photochromic molecule/n-type organic active layer. *J. Mater. Chem. C* **3**, 4156–4161 (2015)

9. Baldo M. A., Holmes R. J. & Forrest S. R. Prospects for electrically pumped organic lasers. *Phys. Rev. B* **66**, 035321 (2002)

10. Nakanotani H., Sasabe H. & Adachi C. Singlet-singlet and singlet-heat annihilations in fluorescence-based organic light-emitting diodes under steady-state high current density. *Appl. Phys. Lett.* **86**, 213506 (2005)

11. Kasemann D., Brückner R., Fröb H. & Leo K. Organic light-emitting diodes under high currents explored by transient electroluminescence on the nanosecond scale, *Phys. Rev. B* **84**, 115208 (2011)